Optimal Battery Dimensioning and Control of a CVT PHEV Powertrain

Nikolce Murgovski, Lars Mårdh Johannesson, *Member, IEEE*, and Bo Egardt, *Fellow, IEEE*

***Abstract*—This paper presents convex modeling steps for the problem of optimal battery dimensioning and control of a plug-in hybrid electric vehicle with a continuous variable transmission. The power limits of the internal combustion engine and the electric machine are approximated as convex/concave functions in kinetic energy, whereas their losses are approximated as convex in both kinetic energy and power. An example of minimizing the total cost of ownership of a city bus including a battery wear model is presented. The proposed method is also used to obtain optimal charging power from an infrastructure that is to be designed at the same time the bus is dimensioned.**

***Index Terms*—Battery sizing, convex optimization, plug-in hybrid electric vehicles (HEVs), power management.**

I. Introduction

DUE to the potential for decreasing fuel consumption and emissions without serious impact on a vehicle's performance, interest in hybrid electric vehicles (HEVs) has grown. HEVs possess most of the features of conventional vehicles; however, in addition to the internal combustion engine (ICE), they also include an energy buffer, typically a battery and/or a super capacitor, and one or more electric machines (EMs). This gives them an additional degree of freedom, allowing for more efficient operation [1]. However, this also makes them more expensive, and to keep the cost down, HEVs may need to include a downsized engine and a carefully selected energy buffer.

The optimal size of the HEV's powertrain components depends on the powertrain configuration, the ability to draw electric energy from the grid, drive patterns, prices of petroleum, electricity and energy buffer, and how well adapted the buffer energy management is to driving conditions. Moreover, the size of the powertrain components and HEV energy management need to be simultaneously optimized because nonoptimal energy management may lead to nonoptimal component sizes [2].

Manuscript received March 16, 2013; revised August 13, 2013 and October 15, 2013; accepted October 31, 2013. Date of publication November 12, 2013; date of current version June 12, 2014. This work was supported in part by the Swedish Energy Agency. The review of this paper was coordinated by Mr. D. Diallo.

N. Murgovski and B. Egardt are with the Department of Signals and Systems, Chalmers University of Technology, Gothenburg 412 96, Sweden (e-mail: nikolce.murgovski@chalmers.se; bo.egardt@chalmers.se).

L. M. Johannesson is with the Department of Signals and Systems, Chalmers University of Technology, Gothenburg 412 96, Sweden, and also with the Viktoria Swedish ICT, Gothenburg 417 56, Sweden (e-mail: larsjo@chalmers.se; lars.johannesson@viktoria.se).

Color versions of one or more of the figures in this paper are available online at http://ieeexplore.ieee.org.

Digital Object Identifier 10.1109/TVT.2013.2290601

The problem of dimensioning and performance assessment of HEV powertrains is mainly approached in the literature by using heuristic methods or dynamic programming (DP) [3]–[9]. These methods typically experience very long computational time for multidimensional problems (with several state variables); as for example, the computational time in DP exponentially increases with the number of state variables [10]. In terms of computational time, a more promising approach has been presented in [11] where convex optimization has been proposed for dimensioning and control of HEVs with either a series or a parallel powertrain topology with a conventional discrete-gear transmission.

Extending the work of Murgovski *et al.* in [11], this study considers a continuous variable transmission (CVT) parallel powertrain for an HEV that has a possibility of drawing electric energy from the grid [a plug-in HEV (PHEV)]. Moreover, the PHEV includes a battery wear model described by a limited energy throughput. The objective is to minimize the total cost of vehicle ownership, which includes a decision on the optimal battery size and energy management that minimizes used fuel, electricity, and number of battery replacements within the lifetime of the vehicle. This is a nonlinear and mixed-integer control problem, where integer variables are the engine on/off control and the number of battery replacements. The problem includes two states, a battery state of charge (SOC) and a CVT gear ratio, and one design parameter, i.e., the battery size.

The contribution of this paper is convex modeling steps that allow a time-efficient suboptimal solution of the PHEV dimensioning problem. Engine on/off control is decided by heuristics, and the remaining subproblem is remodeled as a convex optimization problem that can be solved in several minutes on a standard PC. The power limits of the ICE and the EM are approximated as convex/concave functions in kinetic energy, whereas their losses are approximated as convex in both kinetic energy and power. The short computational time allows the optimization to be repeated for several charging configurations, thus making it possible to optimally design the charging infrastructure at the same time the vehicle is dimensioned.

This paper is outlined as follows. Problem formulation and modeling details are described in Section II, the convex modeling steps are given in Section III, an example of battery dimensioning of a city bus is given in Section IV, the optimal result is validated in Section V, and this paper is ended with discussion and future work in Section VI.

II. Battery Dimensioning Problem

This section describes modeling details and formulates the optimization problem.

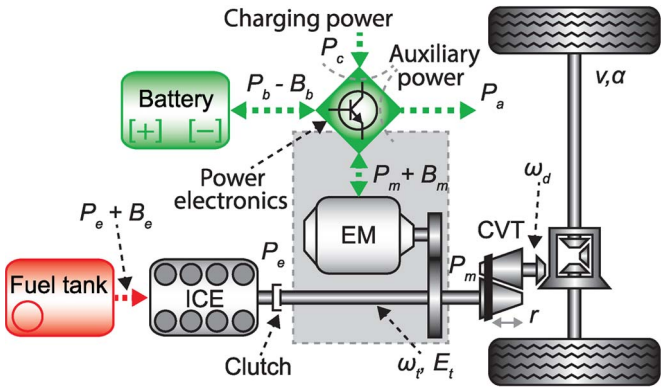

Fig. 1. Parallel PHEV powertrain model with a CVT. The efficiency of the power electronics is averaged and reflected within the EM, the auxiliaries, and the charging stations. The EM speed reduction gear is considered part of the EM.

A. Powertrain Model

We investigate a parallel PHEV powertrain where the ICE and EM are mechanically connected to the wheels through a CVT, as shown in Fig. 1. The vehicle is required to fulfill a certain driving mission fully described by road altitude, desired vehicle velocity, and acceleration at each point in time. In view of the vehicle powertrain, this can be translated to demanded speed $\omega_d(t)$ on the shaft between the differential gear and CVT, and power

$$\boldsymbol{P_m}(t) + \boldsymbol{P_e}(t) = A_1(t) + \boldsymbol{n}A_2(t) + \boldsymbol{P_{brk}}(t) + I(t)\left(\boldsymbol{r^2}(t)\dot{\omega}_d(t)\omega_d(t) + \dot{\boldsymbol{r}}(t)\boldsymbol{r}(t)\omega_d^2(t)\right) \quad (1)$$

that has to be provided by the EM, i.e., $\boldsymbol{P_m}(t)$, or the ICE, i.e., $\boldsymbol{P_e}(t)$. (The optimization variables are marked in bold for readability. As optimization variables, we refer to both the control signals and states in the problem.) The demanded power (detailed in the Appendix) is affine in vehicle mass, and therefore, it is affine in the number of battery cells $\boldsymbol{n}$ that are yet to be determined. The remaining optimization variables in (1) are the power $\boldsymbol{P_{brk}}(t)$ at the friction brakes and the CVT gear ratio $\boldsymbol{r}(t)$. The inertia of the components rotating with speed $\omega_t(\cdot) = \boldsymbol{r}(t)\omega_d(t)$ is denoted by $I(t)$. (The symbol $\cdot$ is used to indicate a function of optimization variables.)

The vehicle's electric path is closed by

$$\boldsymbol{P_c}(t) + \boldsymbol{P_b}(t) = \boldsymbol{P_m}(t) + P_a + B_m(\cdot) + B_b(\cdot) \quad (2)$$

delineating the battery and grid power, i.e., $\boldsymbol{P_b}(t)$ and $\boldsymbol{P_c}(t)$, driving the EM and the auxiliaries, i.e., P_a. Additionally, part of the supplied power is dissipated in the EM and battery (losses), i.e., $B_m(\cdot)$ and $B_b(\cdot)$. We consider positive power when discharging the battery.

The ICE losses, i.e., $B_e(\cdot)$, and the losses of the EM, including losses of the power electronics and the EM gear, are given as static maps [an example is shown later in Fig. 3(a)]. We consider, for simplicity, constant auxiliary power and constant efficiency for the power electronics, CVT, differential gear, and charging stations. The clutch is considered open when the engine is off, and it is therefore identified by the engine on/off state $e(t)$. We assume that the signal $e(t)$ is predecided

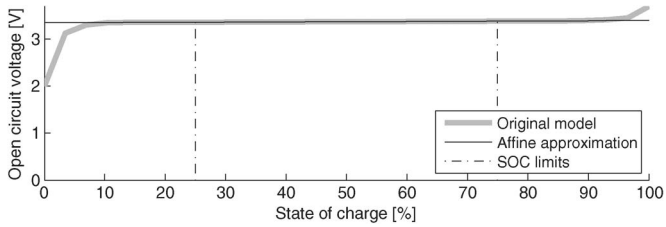

Fig. 2. Battery cell open-circuit voltage.

using heuristics that give suboptimal solutions. This is further discussed in Section IV-A.

The battery consists of $\boldsymbol{n}$ identical cells with open-circuit voltage $u(\cdot)$ that is a nonlinear nonconvex function of the battery SOC, as shown in Fig. 2. Then, the power at the pack terminals, i.e., $\boldsymbol{P_b}(t) - B_b(\cdot)$, is related to the total number of cells, regardless of the configuration (series/parallel). This study is concerned of finding the optimal battery capacity, where $\boldsymbol{n}$ is relaxed to a real number, thus lowering the dependence on premanufactured cells. Instead, we focus on the battery technology, assuming that later, at the manufacturing phase, cells can be fabricated and assembled according to the optimal pack power and capacity.

The battery losses are expressed as

$$B_b(\cdot) = \boldsymbol{n}Ri^2(\cdot) = R\frac{\boldsymbol{P_b^2}(t)}{u^2(\cdot)\boldsymbol{n}} \quad (3)$$

with $i(\cdot)$ and R denoting cell current and resistance, respectively. The SOC derivative is given by

$$\dot{\boldsymbol{s}}(t) = -\frac{i(\cdot)}{Q} = -\frac{\boldsymbol{P_b}(t)}{Qu(\cdot)\boldsymbol{n}} \quad (4)$$

with Q denoting cell capacity.

B. Battery Wear Model

Battery lifetime depends on many factors, e.g., cell's temperature, discharge rate, depth of discharge, charging strategy, amount and frequency of overcharge, etc. [12]. An accurate life prediction model has to consider all these factors to well describe the physical and electrochemical aging processes, both of a single cell and the pack as a whole. However, the complexity of the existing electrochemical models, which entail many states and highly nonlinear electrochemical processes [13], limits their use in problems of assessment and sizing of HEV powertrains.

In a significantly simpler life prediction model, it is assumed that under constant operating conditions, the battery can achieve an overall energy throughput until end of life is reached (capacity fade by 20%). The throughput-based models capture the major battery aging phenomena in HEVs, because battery operation is generally restricted within the linear voltage-SOC region (see Fig. 2), and a battery management system keeps the lumped cell temperature within a certain interval. In the community of HEV's energy management, various weighted throughput models have already been utilized. In [14] and [15], the throughput is parameterized by a charge/discharge rate,

whereas in [16], the dependence on SOC and temperature is also considered.

To lower the computational burden (further discussed in Sections IV and V), we have adopted a simple battery wear model that considers limited battery energy throughput. Denoting the maximum allowed cell's energy throughput by E_{thmax}, the cycled battery energy within the lifetime of the vehicle is limited by

$$\frac{d_v}{d_{dc}} \int_{t_0}^{t_f} |\boldsymbol{P_b}(t)|\, dt \leq (N_r(\cdot)+1)\, \boldsymbol{n} E_{thmax}. \tag{5}$$

The term d_v/d_{dc} gives the number of times the representative driving cycle is driven within the lifetime of the vehicle, where d_v is the average travel distance in the vehicle lifetime, and d_{dc} is the length of the driving cycle. The initial and final time of the driving cycle are denoted by t_0 and t_f. The battery is replaced $N_r(\cdot)$ times within the vehicle lifetime.

C. Nonconvex Optimization Problem

The optimization objective is formulated to minimize the total cost of vehicle ownership. This includes the operational cost for consumed petroleum and electricity, i.e., $J_o(\cdot)$, and battery cost, i.e., $J_b(\cdot)$. The other powertrain components are predetermined and do not enter the cost function. Expressed in [currency/km], these costs are computed as

$$J_o(\cdot) = \frac{1}{d_{dc}} \int_{t_0}^{t_f} \left(w_f \left(\boldsymbol{P_e}(t) + B_e(\cdot) \right) + \frac{w_c}{\eta_c} \boldsymbol{P_c}(t) \right) dt \tag{6}$$

$$J_b(\cdot) = \frac{w_b}{d_v} \left(N_r(\cdot) + 1 \right) \boldsymbol{n} \tag{7}$$

where η_c is the efficiency of the charging stations, w_f and w_c are petroleum and electricity cost in [currency/kWh], and w_b is battery cell cost in [currency] including depreciation expenses. The number of battery replacements can be expressed from (5) as

$$N_r(\cdot) = \text{ceil}\left(\frac{d_v}{d_{dc}} \frac{\int_{t_0}^{t_f} |\boldsymbol{P_b}(t)|\, dt}{\boldsymbol{n} E_{thmax}} \right) - 1 \tag{8}$$

where ceil rounds the value to the nearest integer toward infinity.

The optimization problem can then be summarized as follows:

$$\begin{aligned}
&\text{minimize} \quad J_o(\cdot) + J_b(\cdot) \\
&\text{subject to} \quad (1), (2), (4), \\
&\boldsymbol{P_{brk}}(t) \geq 0 \\
&\boldsymbol{P_e}(t) \in [0, e(t) P_{emax}(\cdot)] && \text{(9a)} \\
&\boldsymbol{P_m}(t) \in [P_{mmin}(\cdot), P_{mmax}(\cdot)] && \text{(9b)} \\
&\boldsymbol{P_c}(t) \in [0, c(t) \eta_c P_{cmax}] && \text{(9c)} \\
&\boldsymbol{P_b}(t) \in [i_{\min}, i_{\max}] u(\cdot) \boldsymbol{n} && \text{(9d)} \\
&\boldsymbol{s}(t) \in [s_{\min}, s_{\max}] && \text{(9e)} \\
&\boldsymbol{s}(t_f) = \boldsymbol{s}(t_0) && \text{(9f)} \\
&\boldsymbol{r}(t) \in [r_{\min}, r_{\max}] && \text{(9g)} \\
&\boldsymbol{n} \geq 0 \\
&t \in [t_0, t_f]
\end{aligned}$$

with $\boldsymbol{P_{brk}}(t)$, $\boldsymbol{P_e}(t)$, $\boldsymbol{P_m}(t)$, $\boldsymbol{P_c}(t)$, $\boldsymbol{P_b}(t)$, $\boldsymbol{s}(t)$, $\boldsymbol{r}(t)$, and $\boldsymbol{n}$ as optimization variables. The constraints include speed-dependent limits on the ICE and EM power [(9a) and (9b), respectively] battery power and SOC limits [(9d) and (9e), respectively], and CVT gear ratio limits (9g). The vehicle can charge with a limited power (9c), only at sections on the driving cycle indicated by $c(t)$. Battery SOC sustaining operation is imposed by (9f).

D. Convex Optimization

A convex problem can be written as

$$\begin{aligned}
&\text{minimize} \quad f_0(\boldsymbol{x}) \\
&\text{subject to} \quad f_i(\boldsymbol{x}) \leq 0 \\
&\qquad\qquad\ \ h_j(\boldsymbol{x}) = 0 \\
&\qquad\qquad\ \ \boldsymbol{x} \in \mathcal{X}
\end{aligned}$$

where $\mathcal{X} \subseteq \mathbb{R}^n$ is a convex set, $f_i(\boldsymbol{x})$ are convex functions, and $h_j(\boldsymbol{x})$ are affine in the vector of optimization variables $\boldsymbol{x}$ [17]. The set of integers is not convex, and this is the reason the engine on/off signal in (9) is decided by heuristics, prior to the optimization. However, (9) is still not convex. This is because of the integer number of battery replacements in (8) and the nonconvex operations in (1), (2), (4), and (9d). Moreover, the ICE and EM losses, i.e., $B_e(\cdot)$ and $B_m(\cdot)$, have to be convex in the optimization variables they depend on. Similarly, the EM generating power limit, i.e., $P_{mmin}(\cdot)$, has to be convex, and the ICE and EM motoring power limits, i.e., $P_{emax}(\cdot)$ and $P_{mmax}(\cdot)$, have to be concave functions.

III. Convex Modeling

This section describes the steps of remodeling problem (9) into a convex optimization problem.

A. Battery

The convex modeling steps to reformulate (3) and (4) have been introduced in [18] and [19] and are only briefly summarized here for consistency.

First, the cell open-circuit voltage is approximated with a linear function

$$u(\cdot) = \frac{Q}{C} \boldsymbol{s}(t) + u_0 \tag{10}$$

as shown in Fig. 2. Second, a variable change is proposed using battery energy

$$\boldsymbol{E_b}(t) = \boldsymbol{n} Q \int_0^{\boldsymbol{s}(t)} u(\cdot) ds(t) = \boldsymbol{n} \frac{C}{2} \left(u^2(\cdot) - u_0^2 \right) \tag{11}$$

instead of SOC. Then, (4), (9d)–(9f) can be written as

$$\dot{\boldsymbol{E}}_{\boldsymbol{b}}(t) = -\boldsymbol{P}_{\boldsymbol{b}}(t) \tag{12}$$

$$\boldsymbol{P}_{\boldsymbol{b}}(t) \in [i_{\min}, i_{\max}]\sqrt{\boldsymbol{n}\left(\frac{2}{C}\boldsymbol{E}_{\boldsymbol{b}}(t) + u_0^2\boldsymbol{n}\right)} \tag{13}$$

$$\boldsymbol{E}_{\boldsymbol{b}}(t) \in \frac{C}{2}\left(\left[u^2(s_{\min}), u^2(s_{\max})\right] - u_0^2\right)\boldsymbol{n} \tag{14}$$

$$\boldsymbol{E}_{\boldsymbol{b}}(t_f) = \boldsymbol{E}_{\boldsymbol{b}}(t_0) \tag{15}$$

where the square root function in (13) is concave in $\boldsymbol{n}$ and $\boldsymbol{E}_{\boldsymbol{b}}(t)$.

Following the steps in [19], a new optimization variable $\boldsymbol{B}_{\boldsymbol{b}}(t)$ is introduced for the battery losses. Then, instead of equality (3), a relaxed constraint is used, i.e.,

$$\boldsymbol{B}_{\boldsymbol{b}}(t) \geq RC\frac{\boldsymbol{P}_{\boldsymbol{b}}^{\boldsymbol{2}}(t)}{2\boldsymbol{E}_{\boldsymbol{b}}(t) + Cu_0^2\boldsymbol{n}} \tag{16}$$

which at the optimum will hold with equality, as otherwise energy will be wasted unnecessarily. The right side of the inequality in (16) is convex in $\boldsymbol{n}$, $\boldsymbol{P}_{\boldsymbol{b}}(t)$, and $\boldsymbol{E}_{\boldsymbol{b}}(t)$.

B. Battery Replacements

To obtain an integer number of battery replacements, we propose a solution in which two slightly modified optimization problems are solved.

P1) First, a convex problem is solved where the number of battery replacements is relaxed to a real number, i.e.,

$$J_b(\cdot) = \frac{w_b}{d_{dc}E_{thmax}}\int_{t_0}^{t_f}|\boldsymbol{P}_{\boldsymbol{b}}(t)|\,dt. \tag{17}$$

Let $\tilde{N}_r^*$ be the optimal number of replacements found by solving the relaxed problem.

P2a) Then, a convex problem is solved where the number of battery replacements in the cost function is fixed to $N_{rmax} = \text{ceil}(\tilde{N}_r^*)$, giving the battery cost

$$J_b(\cdot) = \frac{w_b}{d_v}(N_{rmax} + 1)\boldsymbol{n}. \tag{18}$$

At the same time, a constraint is induced on the energy throughput to ensure that N_{rmax} is not exceeded, which can be written as

$$\int_{t_0}^{t_f}|\boldsymbol{P}_{\boldsymbol{b}}(t)|\,dt \leq \frac{d_{dc}}{d_v}(N_{rmax} + 1)E_{thmax}\boldsymbol{n}. \tag{19}$$

P2b) If $\text{ceil}(\tilde{N}_r^*) > 0$, then the same problem as in P2a) is solved, but with $N_{rmax} = \text{ceil}(\tilde{N}_r^*) - 1$.

The nearest integer to $\tilde{N}_r^*$ that minimizes the total cost in P2a and P2b is chosen as the optimal solution.

C. CVT

Similarly as with the battery, the CVT can be modeled as convex by replacing the gear ratio $\boldsymbol{r}(t)$ with a variable, i.e.,

$$\boldsymbol{E}_{\boldsymbol{t}}(t) = \omega_t^2(\cdot) = \omega_d^2(t)\boldsymbol{r}^{\boldsymbol{2}}(t) \tag{20}$$

expressing nominal kinetic energy of an object with inertia of 2 kgm^2. This will allow (1) to be written as convex, i.e.,

$$\boldsymbol{P}_{\boldsymbol{m}}(t) + \boldsymbol{P}_{\boldsymbol{e}}(t) = A_1(t) + \boldsymbol{n}A_2(t) + \boldsymbol{P}_{\boldsymbol{b}rk}(t) + \frac{I(t)}{2}\dot{\boldsymbol{E}}_{\boldsymbol{t}}(t). \tag{21}$$

Accordingly, constraint (9g) will change to

$$\boldsymbol{E}_{\boldsymbol{t}}(t) \in \left[r_{\min}^2, r_{\max}^2\right]\omega_d^2(t). \tag{22}$$

D. ICE and EM

Due to the variable $\boldsymbol{E}_{\boldsymbol{t}}(t)$ introduced in (20), we seek models for the ICE and EM power limits and losses that are convex (concave for the motoring limits) in $\boldsymbol{E}_{\boldsymbol{t}}(t)$ [i.e., $\omega_t^2(\cdot)$], in addition to $\boldsymbol{P}_{\boldsymbol{e}}(t)$ and $\boldsymbol{P}_{\boldsymbol{m}}(t)$. In the following, we study specific examples of ICE and EM, shown in Fig. 3(a), that will be used later in Section IV.

1) Approximation of Power Limits: A quick investigation of the ICE and EM, shown in the middle row in Fig. 3(a), shows that the power limits are indeed convex/concave in $\omega_t^2(\cdot)$. A straightforward concave approximation of the ICE power limit can be obtained by a piecewise affine function, i.e.,

$$\begin{aligned} P_{emax}(\cdot) &= \min\left\{a_{0j} + a_{1j}\omega_t^2(\cdot)\right\} \\ &= \min\left\{a_{0j} + a_{1j}\boldsymbol{E}_{\boldsymbol{t}}(t)\right\}, \quad j = 1, \ldots, k_e \end{aligned} \tag{23}$$

where we have chosen $k_e = 4$ affine pieces for the model in Fig. 3(b).

Similarly, the EM power limits are approximated with two pieces, i.e., one with constant power and the other with constant torque. Thus

$$P_{mmax}(\cdot) = \min\left\{b_{01}, b_{11}\sqrt{\boldsymbol{E}_{\boldsymbol{t}}(t)}\right\} \tag{24}$$

$$P_{mmin}(\cdot) = \max\left\{b_{02}, b_{12}\sqrt{\boldsymbol{E}_{\boldsymbol{t}}(t)}\right\} \tag{25}$$

where $b_{01}, b_{11} > 0$ and $b_{02}, b_{12} < 0$.

2) Approximation of Power Losses: It is also shown in Fig. 3(a) that the ICE losses, in the nonshaded region, and the EM losses, in the entire region, appear convex in both power and speed squared. When approximating the ICE losses, we disregard the shaded region, because it can be expected that the optimal control will avoid operation at high speeds. This is because for any ICE power, the optimal speed is outside the shaded region [see the optimal efficiency line in Fig. 3(a)], unless a higher speed is enforced by the lower limit of (22). This could happen for very high demanded speed, not typical in normal vehicle operation, and therefore, the misfit in the shaded region will have small influence on the results.

Functions approximating power losses have been found by fitting a second-order polynomial in speed squared, power

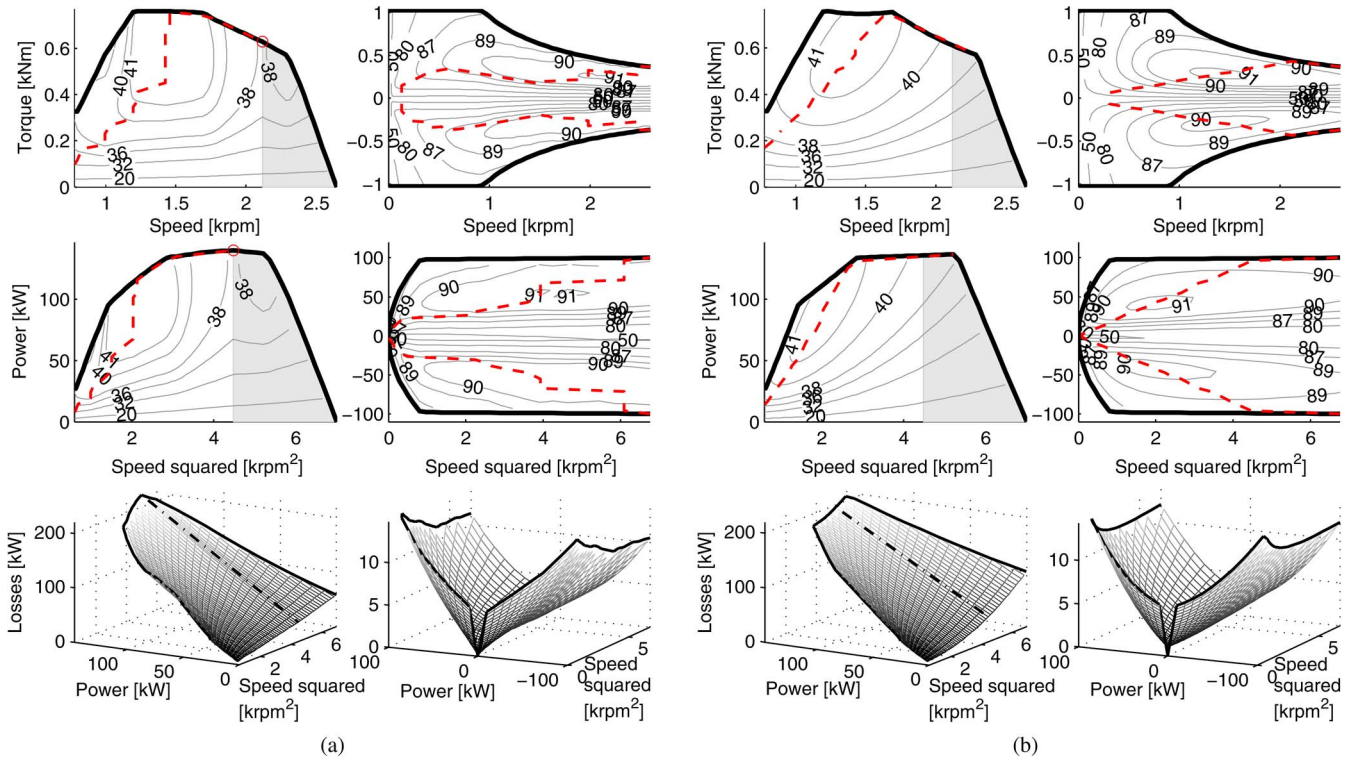

Fig. 3. ICE and EM models. In each subfigure, the ICE model is in the left column, and the EM model is in the right column. The contour lines in the top two rows show efficiency maps, whereas torque/power limits are depicted by the thick solid lines. The dashed lines depict torque-speed points of optimal efficiency for a given demanded power. The shaded region in the top two rows is not considered when approximating the ICE losses. (a) Original models. The circle depicts the point of maximum ICE power. (b) Approximated convex models.

and torque. Similarly as with the battery, new variables are introduced, and the losses are relaxed with inequality, i.e.,

$$\begin{aligned}\boldsymbol{B_e}(t) &\geq e(t)d_0 + d_1\omega_t^4(\cdot) + d_2\boldsymbol{P_e}(t) + d_3\frac{\boldsymbol{P_e^2}(t)}{\omega_t^2(\cdot)}\\ &= e(t)d_0 + d_1\boldsymbol{E_t^2}(t) + d_2\boldsymbol{P_e}(t) + d_3\frac{\boldsymbol{P_e^2}(t)}{\boldsymbol{E_t}(t)} \quad (26)\\ \boldsymbol{B_m}(t) &\geq m(t)g_0 + g_1\omega_t^2(\cdot) + g_2\left|\boldsymbol{P_m}(t)\right|\\ &\quad + g_3\boldsymbol{P_m^2}(t) + g_4\frac{\boldsymbol{P_m^2}(t)}{\omega_t^2(\cdot)}\\ &= m(t)g_0 + g_1\boldsymbol{E_t}(t) + g_2\left|\boldsymbol{P_m}(t)\right|\\ &\quad + g_3\boldsymbol{P_m^2}(t) + g_4\frac{\boldsymbol{P_m^2}(t)}{\boldsymbol{E_t}(t)}. \quad (27)\end{aligned}$$

The coefficients in front of the nonlinear terms are positive, and hence, the losses are convex in $\boldsymbol{P_e}(t)$, $\boldsymbol{P_m}(t)$, and $\boldsymbol{E_t}(t)$. The signals $e(t)$ and $m(t)$ are used to remove the idling losses when the ICE is off and the EM is off and not rotating. Therefore, the EM idling losses are removed when the vehicle speed is zero, i.e.,

$$m(t) = \begin{cases} 0, & \omega_d(t) = 0 \\ 1, & \text{otherwise.} \end{cases} \quad (28)$$

The difference in fuel and electric energy consumption of the original and approximated ICE and EM maps is shown in Fig. 4. It can be noticed that for most of the operating points (excluding the shaded region in the ICE map), the difference is within $[-2, 2]\%$. Further investigation of the accumulated error, after simulating the vehicle against a certain driving cycle, is performed in Section V.

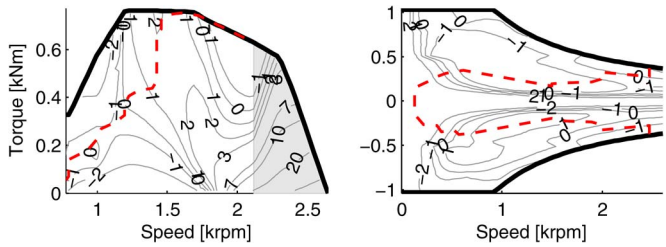

Fig. 4. Difference in (left) fuel and (right) electric energy consumption between operating points of the original and approximated ICE and EM models. The difference between the maps is in percentage, illustrated by the contour lines.

3) Slipping the Clutch: To improve vehicle efficiency, (P)HEVs typically turn the ICE off at low speed and power demands. However, depending on the vehicle and the driving mission, it might be necessary to keep the ICE on at certain time instances where the speed $\omega_t(\cdot)$ has to drop below the ICE idling speed. In an actual vehicle, this can be achieved by, e.g., slipping the clutch. However, it can be easily concluded that the convex ICE model will not allow ICE operation at very low speed, and even one such time instance will yield the optimization problem infeasible. This is easier to investigate if the ICE and the slipping clutch are considered as one unit, as in Fig. 5. The maximum power of this unit is not concave in $\omega_t^2(\cdot)$, and the concave approximation (23) will not allow ICE operation left of the dashed line in Fig. 5.

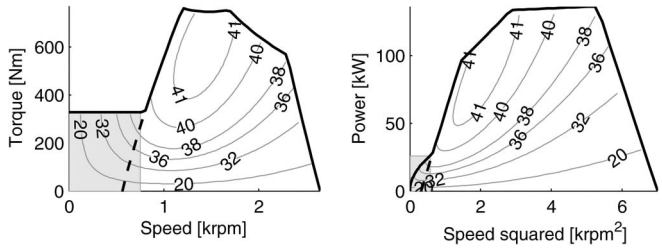

Fig. 5. ICE and the clutch as a single unit. The clutch is slipping when operating within the shaded region.

A solution to this problem, which does not infringe convexity, can be obtained by switching the ICE model based on a known signal, e.g., $\omega_d(t)$. Each time $\omega_d(t)$ drops below a threshold ω_{slipp}, the ICE power will be limited by

$$P_{emax}(\cdot) = T_{emax}(\omega_{idle})\sqrt{\boldsymbol{E_t}(t)} \tag{29}$$

instead of (23). The torque $T_{emax}(\omega_{idle})$ is the maximum torque the ICE can deliver at idling speed.

While slipping the clutch, within the shaded region in Fig. 5, the CVT gear ratio has to be high. Therefore, the threshold ω_{slipp} can be found as

$$\omega_{slipp} = \frac{\omega_{idle}}{r_{\max} - \epsilon} \tag{30}$$

where ϵ is a small positive number that can be used to allow limited freedom in the choice of gear. If, instead, it is assumed that the CVT must have the highest gearing, then ϵ can be set to zero, and (29) can be simplified to

$$P_{emax}(\cdot) = T_{emax}(\omega_{idle})\omega_d(t) r_{\max}. \tag{31}$$

The ICE losses (26) can also be replaced by any other function convex in $\boldsymbol{P_e}(t)$ and $\boldsymbol{E_t}(t)$ when the clutch is slipping. In the rest of this paper, we have chosen the same losses (26) for the whole speed range.

Finally, the convex optimization problem can be summarized as in Table I.

TABLE I
CONVEX OPTIMIZATION PROBLEM

minimize

$$J_o(\boldsymbol{P_e}(t), \boldsymbol{B_e}(t), \boldsymbol{P_c}(t)) + \begin{cases} \frac{w_b}{d_{dc} E_{thmax}} \int_{t_0}^{t_f} |\boldsymbol{P_b}(t)|\, dt, & \text{case P1} \\ \frac{w_b}{d_v}(N_{rmax}+1)\boldsymbol{n}, & \text{case P2} \end{cases}$$

subject to

$$\boldsymbol{P_m}(t) + \boldsymbol{P_e}(t) = A_1(t) + \boldsymbol{n}A_2(t) + \boldsymbol{P_{brk}}(t) + \tfrac{I(t)}{2}\dot{\boldsymbol{E}}_{\boldsymbol{t}}(t)$$
$$\boldsymbol{P_c}(t) + \boldsymbol{P_b}(t) = \boldsymbol{P_m}(t) + P_a + \boldsymbol{B_m}(t) + \boldsymbol{B_b}(t)$$
$$\boldsymbol{B_b}(t) \geq RC\frac{\boldsymbol{P_b^2}(t)}{2\boldsymbol{E_b}(t) + Cu_0^2\boldsymbol{n}}$$
$$\boldsymbol{B_e}(t) \geq e(t)d_0 + d_1\boldsymbol{E_t^2}(t) + d_2\boldsymbol{P_e}(t) + d_3\frac{\boldsymbol{P_e^2}(t)}{\boldsymbol{E_t}(t)}$$
$$\boldsymbol{B_m}(t) \geq m(t)g_0 + g_1\boldsymbol{E_t}(t) + g_2|\boldsymbol{P_m}(t)| + g_3\boldsymbol{P_m^2}(t) + g_4\frac{\boldsymbol{P_m^2}(t)}{\boldsymbol{E_t}(t)}$$
$$\boldsymbol{P_{brk}}(t) \leq 0$$
$$\boldsymbol{P_e}(t) \in \begin{cases} [0, e(t)\min\{a_{0j} + a_{1j}\boldsymbol{E_t}(t)\}], & \omega_d(t) > w_{slipp}, \\ \left[0, e(t)T_{emax}(\omega_{idle})\sqrt{\boldsymbol{E_t}(t)}\right], & \omega_d(t) \leq w_{slipp} \end{cases}$$
$$\boldsymbol{P_m}(t) \in m(t)\left[\max\left\{b_{02}, b_{12}\sqrt{\boldsymbol{E_t}(t)}\right\}, \min\left\{b_{01}, b_{11}\sqrt{\boldsymbol{E_t}(t)}\right\}\right]$$
$$\boldsymbol{P_c}(t) \in [0, c(t)\eta_c P_{cmax}]$$
$$\boldsymbol{P_b}(t) \in [i_{min}, i_{max}]\sqrt{\boldsymbol{n}\left(\tfrac{2}{C}\boldsymbol{E_b}(t) + u_0^2\boldsymbol{n}\right)}$$
$$\dot{\boldsymbol{E}}_{\boldsymbol{b}}(t) = -\boldsymbol{P_b}(t)$$
$$\boldsymbol{E_b}(t) \in \tfrac{C}{2}\left(\left[u^2(s_{min}), u^2(s_{max})\right] - u_0^2\right)\boldsymbol{n}$$
$$\boldsymbol{E_b}(t_f) = \boldsymbol{E_b}(t_0)$$
$$\boldsymbol{E_t}(t) \in [r_{min}^2, r_{max}^2]\omega_d^2(t)$$
$$\boldsymbol{n} \geq 0$$
$$\int_{t_0}^{t_f} |\boldsymbol{P_b}(t)|dt \leq \begin{cases} +\infty, & \text{case P1} \\ \frac{d_{dc}}{d_v}(N_{rmax}+1)E_{thmax}\boldsymbol{n}, & \text{case P2} \end{cases}$$
$$t \in [t_0, t_f], \quad j = 1, ..., k_e$$

Optimization variables are: $\boldsymbol{P_{brk}}(t), \boldsymbol{P_e}(t), \boldsymbol{P_m}(t), \boldsymbol{P_c}(t), \boldsymbol{P_b}(t), \boldsymbol{B_e}(t), \boldsymbol{B_m}(t), \boldsymbol{B_b}(t), \boldsymbol{E_b}(t), \boldsymbol{E_t}(t), \boldsymbol{n}$.

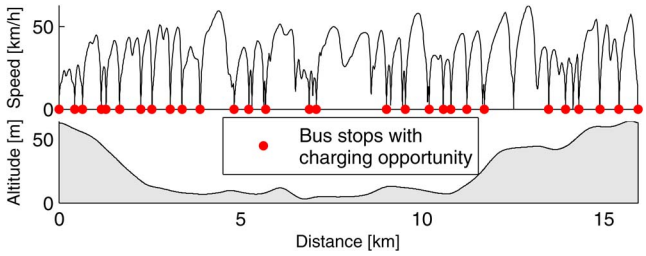

Fig. 6. Bus line with charging opportunities. The bus starts and ends the route at the same bus stop.

IV. OPTIMIZATION EXAMPLE

This section gives an example of optimal battery dimensioning of a plug-in hybrid electric city bus. The bus is driven on a bus line that has opportunity of installing charging stations on 28 bus stops, as shown in Fig. 6. The charging infrastructure is to be developed at the same time the bus is dimensioned, and we are interested in finding the optimal battery versus number of stations, assuming that the bus cannot stay (charge) longer than 20 s at the bus stops. Moreover, it is of interest to find the optimal magnitude of charging power versus number of stations, if the absolute maximum a charging station can provide is 250 kW.

The bus is equipped with 135-kW Diesel ICE and ±100-kW EM, as shown in Fig. 3(a). The battery cell, i.e., ANR26650M1, is a high-power lithium-ion cell from A123 Systems (Westborough, MA, USA). The value for the energy throughput is based on experimental data of the cell operated under constant conditions [12], [20]. Depending on temperature, charge/discharge rate, and depth of discharge, the battery throughput may vary from about 2000 to 20 000 Ah. A PHEV is typically not operated under constant conditions and is very likely to utilize the battery in relatively high charge/discharge rates. Nevertheless, we have chosen an optimistic value of 16 800 Ah, and considering the nearly constant open-circuit voltage, the cell's energy throughput is rounded to 55.4 kWh.

The allowed SOC range is within 25%–75%, and the operation is charge sustaining with free final SOC.

A. Engine On/Off Control

We have adopted a heuristic engine on/off control strategy that has been proposed in [11]. The strategy is based on the knowledge that the engine is most efficient at high torque and medium speed, as shown in Fig. 3(a). Thus, ICE operation at low power demand is avoided. Each time the power of the

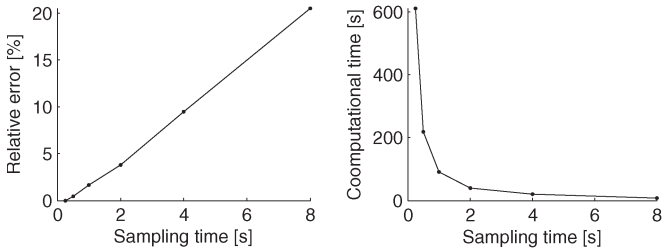

Fig. 7. (Left) Relative error in total cost and (right) computational time versus sampling time. The values are averaged over the different charging configurations. The baseline cost is obtained with 0.25-s sampling time.

baseline vehicle (battery with n_{base} cells) exceeds threshold P_{on}^*, the engine is turned on, i.e.,

$$e(t) = \begin{cases} 1, & A_1(t) + n_{base} A_2(t) > P_{on}^* \\ 0, & \text{otherwise.} \end{cases} \tag{32}$$

The optimal power threshold P_{on}^* is found by iteratively solving the convex problem for several gridded (discrete) thresholds within the power range of the vehicle. The threshold is also recomputed for the different charging configurations.

B. Sampling Time

The convex optimization problem is written in discrete time using first-order Euler discretization (see, e.g., [11]). Then, a package is used, i.e., CVX [21], [22], to translate the problem into a form required by the solver, i.e., SeDuMi [23]. The problem is nonlinear second-order cone [17], where the number of variables depends on the sampling time, because in the discrete domain, each time-dependent variable becomes a vector of optimization variables (a variable per time instance).

We have investigated sampling time from 0.25 to 8 s, while running the code on a standard PC (4-GB RAM, 2.67-GHz dual-core CPU). The computational time and relative error in total cost are given in Fig. 7, where the baseline cost is obtained with 0.25-s sampling. To keep the computational time down, less than 100 s, the remaining results in this paper are obtained with 1-s sampling time. This gives a relative error in total cost of about 2%.

C. Optimal Battery Size and Charging Power

One of the questions this work investigates is whether the inclusion of the battery wear model brings significant changes to the optimal battery size and PHEV energy management. For this reason, we show the optimal results in Fig. 8 for a battery model with unlimited energy throughput and a model with limited throughput.

When energy throughput is not limited, we observe similar results to those published in [24]. The battery size first increases with the number of charging stations to make room for the available grid energy, thus charging with full grid power. At the same time, the vehicle is increasingly driven on electric power, and the cost for consumed diesel fuel decreases. When the number of charging stations reaches 14, the vehicle is capable of being driven almost entirely on electric power. With greater number of stations, the battery size starts to decrease as well

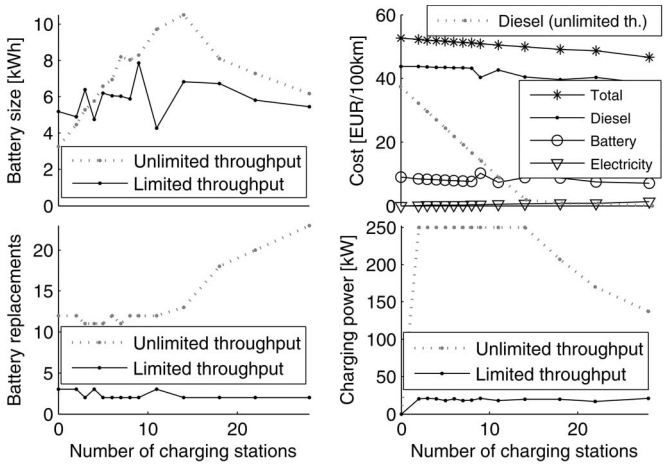

Fig. 8. Optimal results versus charging configuration. The dotted line in the bottom-left plot shows the number of battery replacements that would be needed, if the limit on throughput is applied after the optimization has finished.

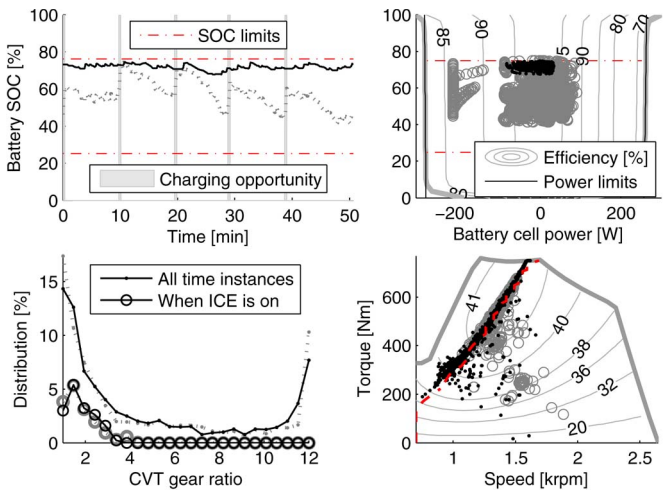

Fig. 9. Optimal results for an infrastructure with five charging stations. The solid lines, in the left column, show results for the battery model with limited energy throughput. The dotted lines show the corresponding results (same marker), but for a battery with unlimited throughput. The optimal operating points, in the right column, are shown with dot markers for the battery with limited throughput and with circles for the battery with unlimited throughput.

as the average charging grid power. However, this operation requires a significant amount of cycled battery energy. If the limit on energy throughput is applied after the optimization has finished, the battery would need more than 20 replacements within the lifetime of the vehicle.

When the limit on energy throughput is considered in the optimization, the results are noticeably different. In this case, the battery size is about 6 kWh (entire energy content) regardless of the number of charging stations. Furthermore, the optimization refocuses on lowering the cycled battery energy, resulting in grid charging power of less than 25 kW and requiring no more than three pack replacements.

D. Optimal Energy Management

To investigate the optimal energy management in more detail, we have chosen one specific configuration with five charging stations. The results are shown in Fig. 9.

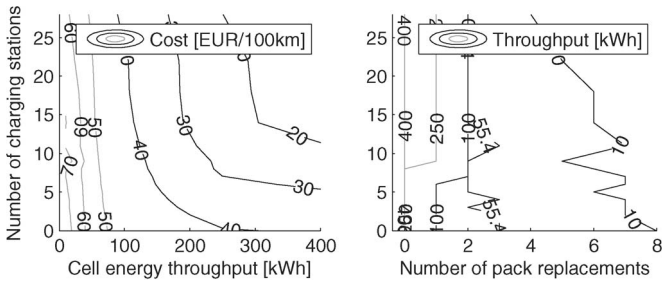

Fig. 10. (Left plot) Optimization cost and (right plot) number of battery pack replacements versus number of charging stations and limits on cell energy throughput.

When energy throughput is not limited, the battery uses most of its available SOC range. The optimization has sized the battery to allow cell operation mainly at greater than 90% efficiency, except during brake regeneration and grid charging, when operation at lower efficiency is also taking place. When energy throughput is limited, the battery does not use more than 10% SOC, and the operation is kept within the 90% efficiency region. To further reduce losses, the operating points are located closer to the upper SOC limit where the open-circuit voltage is slightly higher.

The optimal distribution of the CVT gear ratio is similar in the two cases. When the ICE is on, the optimal gear ratio is typically low, thus allowing the ICE to operate at higher torque. When operating in electric mode, high gear ratio is also common, thus allowing the EM to operate at high speed and low torque. The ICE operating points, shown in the bottom-right plot in Fig. 9, are scattered mainly along the optimal efficiency line.

E. Influence of Cell Energy Throughput

In Fig. 10, we show the influence of cell energy throughput on the total optimization cost and the number of pack replacements. We vary the limit on cell energy throughput in the interval 10–400 kWh, while assuming, for simplicity, that the cell price and all remaining parameters stay unchanged.

The results could be used to indicate a more suitable battery cell for the studied application. For example, if a hybrid electric bus (not plug-in) is requested to cost about 40 EUR/100 km (operational and battery cost), then a battery cell has to be chosen with about 300 kWh of energy throughput. If the bus is plug-in and the infrastructure is equipped with charging stations on all bus stops, then the same cost can be reached using a cell with about 100 kWh of throughput. If the plug-in bus is requested to cost about 30 EUR/100 km, then the bus line should be equipped with at least five charging stations, regardless of the cell's throughput. A demand to never replace the battery within a lifetime period of five years of the non-plug-in bus can be reached by choosing a cell with energy throughput of about 250 kWh or higher.

V. Validation With Dynamic Programming

The difference from the globally optimal solution is validated by comparing results with those obtained by DP. The comparison is performed only on a subproblem of (9), in which battery wear is not included, battery size is kept constant, and the final battery SOC (and, consequently, the initial SOC) is not free. The reason for doing this is to keep the computational time down. Recall that in DP, the computational time is exponential to the number of states, and (9) has two states, SOC and CVT gear ratio, and a design parameter, i.e., battery size, which can be considered a third state. Moreover, the ceil function in the objective or the limit on battery replacements will require an additional state for energy throughput. Additional DP iterations are also needed to allow free final SOC while sustaining the initial charge. In terms of computational effort, this corresponds to including a fifth state in the problem.

In effect, the considered subproblem requires only two states, SOC and CVT gear ratio. Furthermore, to emphasize validation of the ICE model approximation, an infrastructure is considered without charging opportunities, which promotes longer ICE operation. Then, the objective function is simply formulated to minimize fuel consumption.

We apply Bellman's principle of optimality, i.e., [10], to solve the problem via backward recursion. Denoting with $J^*_{DP}(s(t_k), r(t_k), t_k)$ the cost matrix holding the optimal cost-to-go from states $s(t_k)$ and $r(t_k)$ to the desired final state at time t_f, the optimization problem, at time instance t_k, can be formulated as follows:

$$
\begin{aligned}
&J^*_{DP}\left(s(t_k), r(t_k), t_k\right) \\
&\quad = \min_{z_r(t_k), T_e(t_k)} \{T_e(t_k) r(t_k) \omega_d(t_k) \Delta t \\
&\qquad\qquad + J^*_{DP}(s(t_{k+1}), r(t_{k+1}), t_{k+1})\} \\
&\text{s.t.} : (1), (2), (4), (9\text{b}), (9\text{d}) \text{ at } t_k, \\
&s(t_k) \in \mathcal{S} \subseteq [s_{\min}, s_{\max}] \\
&r(t_k) \in \mathcal{R}(t_k) \subseteq [r_{\min}, R_{\max}(t_k)] \\
&T_e(t_k) \in \mathcal{T}_e \subseteq [0, T_{emax}] \\
&z_r(t_k) \in \mathcal{R}(t_{k+1}) \subseteq [r_{\min}, R_{\max}(t_{k+1})] \\
&t_k \in \mathcal{T} \subseteq [t_0, t_f].
\end{aligned}
$$

Control signals are the engine torque $T_e(t_k)$ and the desired gear ratio at the next time instant, i.e., $z_r(t_k) = r(t_{k+1})$. The cost at the final time is a penalty for violating the battery-charge-sustaining constraint. We chose a linear penalty function, i.e.,

$$J^*_{DP}\left(s(t_f), r(t_f), t_f\right) = 1000 \cdot |s(t_f) - s_0| .$$

Discrete values are used for the states and control signals, and the derivatives are replaced with a difference. The grid resolution of the discrete sets, i.e., $\mathcal{T}, \mathcal{S}, \mathcal{R}(t_k)$, and $\mathcal{T}_e$, determines the accuracy of the solution. The same sampling time $\Delta t = 1$ s has been used as in the convex problem, whereas the number of grid points for the remaining discrete sets has been varied from 21 to 101, uniformly spaced within the signals' boundaries. To avoid infeasibility when using a sparse grid, the set $\mathcal{R}(t_k)$ has been varied at each time instant, such that it contains the same

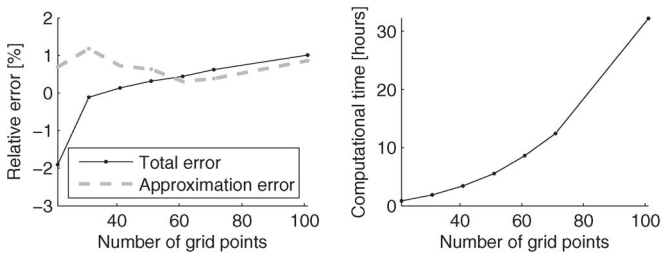

Fig. 11. Solid line in the left plot shows the relative difference in fuel consumption between the optimal fuel consumption obtained by convex optimization and the global optimum obtained by DP. The dashed line shows the difference in fuel consumption due to utilization of approximated ICE, EM, and battery model. The right plot shows the computational time of DP versus number of grid points for the discrete state and input spaces.

number of grid points within the interval $[r_{\min}, R_{\max}(t_k)]$. The upper limit on gear ratio $R_{\max}(t_k)$ is computed as

$$R_{\max}(t_k) = \begin{cases} \min\left\{r_{\max}, w_{tmax}/w_d(t_k)\right\}, & w_d(t_k) > 0 \\ r_{\max}, & w_d(t_k) = 0 \end{cases}$$

where w_{tmax} is the maximum speed the ICE and EM can deliver.

The validation results for a 4.5-kWh battery (entire energy content) and SOC initialized to 50% are shown in Fig. 11. The difference in fuel consumption is expressed as a relative error, i.e.,

$$\frac{\text{Fuel cons. convex} - \text{Fuel cons. DP}}{\text{Fuel cons. DP}} \times 100.$$

It can be observed that when using a sparse grid, the convex optimization is actually more accurate than DP (look for the negative error in Fig. 11). For a grid with 101 points, a more accurate result is obtained, showing improvement in fuel consumption by 1.01%; however, the price to pay is more than 30 h of computational time. The results coincide with those published in [25], where it has been observed that the error due to the on/off heuristics (32) is on the order of 1%, and typically lower.

The error induced by approximations has been investigated by comparing the global optimum of DP with the optimum of another instance of DP evaluated with the approximated ICE, EM, and battery models. The results are presented in Fig. 11, showing an average error that is less than 1%, which at 101 grid points is 0.86%. The approximation error has also been investigated by mapping the optimal ICE operating points from the convex optimization to the original ICE model. This gave a fuel consumption error of 0.82%, averaged over the different charging configurations.

VI. Discussion and Future Work

In addition to the presented method for optimal battery dimensioning and power-split control of a CVT PHEV powertrain, we provide some aspects concerning problem pretreatment, and we discuss future work.

A. Numerical Challenges and Pretreatment

With the chosen driving cycle, the optimization problem has a moderate size even when the sampling time is 0.25 s. (SeDuMi, which solves the dual problem for improved efficiency, reports 470 000 variables and 170 000 equality constraints.) However, the optimization will require long computational time and may be subject to numerical challenges that would arise for long driving cycles, when, e.g., the bus is to be driven on several bus lines.

In this paper, several measures have been taken to shorten the computational time. The braking power, which is a slack variable, has been taken outside the optimization by relaxing the equality in (21) with inequality (see [11] for details). The variables constrained to a certain value have also been removed from the optimization. For example, the grid, ICE and EM power (and losses), may be nonzero only at time instances with a charging opportunity or when $e(t) = 1$ and $m(t) = 1$, respectively. All variables are scaled so that their values belong to a similar range.

One of the most important preprocessing steps is writing the problem in a sparse matrix form [17]. In this paper, we allowed CVX to decide on the problem sparsity, while special attention to this topic will be paid in future studies.

B. Future Work

Despite using a very simple battery wear model, this study indicated that completely omitting a wear model may cause unrealistic sizing of (P)HEV powertrains. This motivates future studies incorporating a more detailed battery wear model. Some steps in this direction have already been taken in [15], where it has been shown that it is possible to include a c-rate-dependent throughput-based battery wear model in convex optimization. Further studies will investigate the possibility of including the dependence on other factors, such as depth of discharge and temperature.

Future studies may focus on applying the method to longer driving cycles using distributed optimization [26]. Improved ICE on/off control and a generalization of the ICE and EM approximations is a major topic to be also considered in future studies.

Appendix
Data and Modeling

Given the longitudinal vehicle velocity $v(t)$ and road gradient $\alpha(t)$, the dissipative forces the vehicle encounters are the aerodynamic drag and the rolling resistance, i.e.,

$$F_a(t) = \frac{\rho_a A_f c_d}{2} v^2(t), \quad F_r(t) = m_t(\boldsymbol{n}) g c_r \cos\alpha(t).$$

Then, the mechanical power balance equation is

$$\begin{aligned} &\left(\left(\frac{I_v}{r_w^2} + m_t(\boldsymbol{n})\right)\dot{v}(t) + m_t(\boldsymbol{n}) g \sin\alpha(t)\right) v(t) \\ &\quad + \left(F_a(t) + F_r(t)\right) v(t) = \left(\eta_d \eta_t\right)^{\operatorname{sgn}\dot{v}(t)} \left(\boldsymbol{P_m}(t) + \boldsymbol{P_e}(t)\right) \\ &\quad - \eta_d^{\operatorname{sgn}\dot{v}(t)} \left(I_t + \eta_t^{\operatorname{sgn}\dot{v}(t)} \left(I_m + I_e e(t)\right)\right) \\ &\quad \times \left(\boldsymbol{r^2}(t)\dot{\omega}_d(t)\omega_d(t) + \dot{\boldsymbol{r}}(t)\boldsymbol{r}(t)\omega_d^2(t)\right) - \tilde{\boldsymbol{P}}_{\boldsymbol{b}rk}(t). \end{aligned}$$

TABLE II
PARAMETER VALUES

Vehicle frontal area	$A_f = 7.54\,\mathrm{m}^2$
Aerodynamic drag coefficient	$c_d = 0.7$
Rolling resistance coefficient	$c_r = 0.007$
Air density	$\rho_a = 1.184\,\mathrm{kg/m}^3$
Wheel radius	$r_w = 0.509\,\mathrm{m}$
Differential gear ratio	$r_d = 4.7$
Vehicle mass without the battery	$m_v = 14.5\,\mathrm{t}$
Battery cell mass	$m_c = 70\,\mathrm{g}$
Inertia of differential gear and wheels	$I_v = 80\,\mathrm{kgm}^2$
Inertia of EM and speed reduction gear	$I_m = 2.37\,\mathrm{kgm}^2$
ICE inertia	$I_e = 1.5\,\mathrm{kgm}^2$
CVT inertia	$I_t = 1\,\mathrm{kgm}^2$
CVT efficiency	$\eta_t = 95\,\%$
Differential gear efficiency	$\eta_d = 95\,\%$
Battery price	1500 EUR/kWh
$Q = 2.3\,\mathrm{Ah}$, $i_{max} = 120\,\mathrm{A}$, $i_{min} = -70\,\mathrm{A}$, $R = 10\,\mathrm{m}\Omega$, $r_{min} = 1$, $r_{max} = 12$, $P_a = 7\,\mathrm{kW}$, $\eta_c = 92\,\%$, $d_v = 400\,000\,\mathrm{km}$, $w_f = 0.154\,\mathrm{EUR/kWh}$, $w_c = 0.06\,\mathrm{EUR/kWh}$, $w_b = 13.09\,\mathrm{EUR}$	

After applying the following changes:

$$m_t(\boldsymbol{n}) = m_v + \boldsymbol{n} m_c, \quad \omega_d(t) = r_d \frac{v(t)}{r_w}$$

$$A_2(t) = m_c \frac{v(t)\left(g c_r \cos\alpha(t) + g \sin\alpha(t) + \dot{v}(t)\right)}{(\eta_d \eta_t)^{\mathrm{sgn}\dot{v}(t)}}$$

$$A_1(t) = \frac{m_v}{m_c} A_2(t) + v(t) \frac{F_a(t) + I_v \frac{\dot{v}(t)}{r_w^2}}{(\eta_d \eta_t)^{\mathrm{sgn}\dot{v}(t)}}$$

$$\boldsymbol{P}_{\boldsymbol{b}rk}(t) = \frac{\tilde{\boldsymbol{P}}_{\boldsymbol{b}rk}(t)}{(\eta_d \eta_t)^{\mathrm{sgn}\dot{v}(t)}}, \quad I(t) = \frac{I_t}{\eta_t^{\mathrm{sgn}\dot{v}(t)}} + I_m + I_e e(t)$$

the form that has been used in (1) can be obtained. Parameter values are given in Table II. The battery depreciation expenses are as described in [11].

ACKNOWLEDGMENT

The authors would like to thank Dr. J. Hellgren and Dr. E. Gelso for their support on testing an instance of this method within AB Volvo.

REFERENCES

[1] L. Guzzella and A. Sciarretta, *Vehicle Propulsion Systems*, 3rd ed. Berlin, Germany: Springer-Verlag, 2013.
[2] T. C. Moore, "HEV control strategy: Implications of performance criteria, system configuration and design, and component selection," in *Proc. Amer. Control Conf.*, Albuquerque, NM, USA, Jun. 1997, pp. 679–683.
[3] U. Zoelch and D. Schroeder, "Dynamic optimization method for design and rating of the components of a hybrid vehicle," *Int. J. Veh. Des.*, vol. 19, no. 1, pp. 1–13, 1998.
[4] S. M. Lukic and A. Emadi, "Effects of drivetrain hybridization on fuel economy and dynamic performance of parallel hybrid electric vehicles," *IEEE Trans. Veh. Technol.*, vol. 53, no. 2, pp. 385–389, Mar. 2004.
[5] M. Kim and H. Peng, "Power management and design optimization of fuel cell/battery hybrid vehicles," *J. Power Sources*, vol. 165, no. 2, pp. 819–832, Mar. 2007.
[6] O. Sundström, L. Guzzella, and P. Soltic, "Torque-assist hybrid electric powertrain sizing: From optimal control towards a sizing law," *IEEE Trans. Control Syst. Technol.*, vol. 18, no. 4, pp. 837–849, Jul. 2010.
[7] S. J. Moura, D. S. Callaway, H. K. Fathy, and J. L. Stein, "Tradeoffs between battery energy capacity and stochastic optimal power management in plug-in hybrid electric vehicles," *J. Power Sources*, vol. 195, no. 9, pp. 2979–2988, May 2010.
[8] N. Murgovski, J. Sjöberg, and J. Fredriksson, "A methodology and a tool for evaluating hybrid electric powertrain configurations," *Int. J. Elect. Hybrid Veh.*, vol. 3, no. 3, pp. 219–245, Jan. 2011.
[9] S. Ebbesen, C. Dönitz, and L. Guzzella, "Particle swarm optimisation for hybrid electric drive-train sizing," *Int. J. Veh. Des.*, vol. 58, no. 2–4, pp. 181–199, Jun. 2012.
[10] R. Bellman, *Dynamic Programming*. Princeton, NJ, USA: Princeton Univ. Press, Jun. 1957.
[11] N. Murgovski, L. Johannesson, J. Sjöberg, and B. Egardt, "Component sizing of a plug-in hybrid electric powertrain via convex optimization," *Mechatronics*, vol. 22, no. 1, pp. 106–120, Feb. 2012.
[12] J. Wang, P. Liu, J. Hicks-Garner, E. Sherman, S. Soukiazian, M. Verbrugge, H. Tataria, J. Musser, and P. Finamore, "Cycle-life model for graphite- $LiFePO_4$ cells," *J. Power Sources*, vol. 196, no. 8, pp. 3942–3948, Apr. 2011.
[13] D. U. Sauer and H. Wenzl, "Comparison of different approaches for lifetime prediction of electrochemical systems—Using lead-acid batteries as example," *J. Power Sources*, vol. 176, no. 2, pp. 534–546, Feb. 2008.
[14] S. Ebbesen, P. Elbert, and L. Guzzella, "Battery state-of-health perceptive energy management for hybrid electric vehicles," *IEEE Trans. Veh. Technol.*, vol. 61, no. 7, pp. 2893–2900, Sep. 2012.
[15] L. Johannesson, N. Murgovski, S. Ebbessen, B. Egardt, E. Gelso, and J. Hellgren, "Including a battery state of health model in the HEV component sizing and optimal control problem," in *Proc. IFAC Symp. Adv. Autom. Control*, Tokyo, Japan, 2013, pp. 398–403.
[16] L. Serrao, S. Onori, A. Sciarretta, Y. Guezennec, and G. Rizzoni, "Optimal energy management of hybrid electric vehicles including battery aging," in *Proc. ACC*, San Francisco, CA, USA, 2011, pp. 2125–2130.
[17] S. Boyd and L. Vandenberghe, *Convex Optimization*. Cambridge, U.K.: Cambridge Univ. Press, 2004.
[18] N. Murgovski, L. Johannesson, and J. Sjöberg, "Convex modeling of energy buffers in power control applications," in *Proc. IFAC Workshop E-CoSM*, Paris, France, Oct. 23–25, 2012, pp. 92–99.
[19] N. Murgovski, L. Johannesson, A. Grauers, and J. Sjöberg, "Dimensioning and control of a thermally constrained double buffer plug-in HEV powertrain," in *Proc. 51st IEEE Conf. Decision Control*, Maui, HI, Dec. 10–13, 2012, pp. 6346–6351.
[20] S. B. Peterson, J. Apt, and J. Whitacre, "Lithium-ion battery cell degradation resulting from realistic vehicle and vehicle-to-grid utilization," *J. Power Sources*, vol. 195, no. 8, pp. 2385–2392, Apr. 2010.
[21] CVX: Matlab Software for Disciplined Convex Programming, ver. 2.0 beta, CVX Research Inc., Austin, TX, USA, Sep. 2012. [Online]. Available: http://cvxr.com/cvx
[22] M. Grant and S. Boyd, "Graph implementations for nonsmooth convex programs," in *Recent Advances in Learning and Control*, V. Blondel, S. Boyd, and H. Kimura, Eds. Berlin, Germany: Springer-Verlag, 2008, pp. 95–110. [Online]. Available: http://stanford.edu/~boyd/graph_dcp.html
[23] Y. Labit, D. Peaucelle, and D. Henrion, "SeDuMi interface 1.02: A tool for solving LMI problems with SeDuMi," in *Proc. IEEE Int. Symp. Comput. Aided Control Syst. Des.*, Sep. 2002, pp. 272–277.
[24] N. Murgovski, L. Johannesson, J. Hellgren, B. Egardt, and J. Sjöberg, "Convex optimization of charging infrastructure design and component sizing of a plug-in series HEV powertrain," in *Proc. IFAC World Congr.*, Milan, Italy, 2011, pp. 13 052–13 057.
[25] N. Murgovski, L. Johannesson, and J. Sjöberg, "Engine on/off control for dimensioning hybrid electric powertrains via convex optimization," *IEEE Trans. Veh. Technol.*, vol. 62, no. 7, pp. 2949–2962, Sep. 2013.
[26] S. Boyd, N. Parikh, and E. Chu, *Distributed Optimization and Statistical Learning via the Alternating Direction Method of Multipliers*. Delft, The Netherlands: Now, 2011.

Nikolce Murgovski received the M.Sc. degree in software engineering from University West, Stockholm, Sweden, in 2007 and the M.Sc. degree in applied physics and the Ph.D. degree in signals and systems from Chalmers University of Technology, Gothenburg, Sweden, in 2007 and 2012, respectively.

He is currently a Postdoctoral Researcher with the Department of Signals and Systems, Chalmers University of Technology. His research interests include optimal control and dimensioning of automotive powertrains.

Lars Mårdh Johannesson (M'12) received the M.Sc. degree in automation and mechatronics and the Ph.D. degree in automatic control from Chalmers University of Technology, Gothenburg, Sweden, in 2004 and 2009, respectively.

Since 2011, he has been with the Electromobility Group, Viktoria Swedish ICT, Gothenburg, researching powertrain control within the Chalmers Energy Initiative. His main research interests include optimal control of hybrid and plug-in hybrid electric vehicles, control of auxiliary systems in trucks, active cell balancing, and system studies of hybrid vehicles.

Bo Egardt (SM'90–F'03) received the M.Sc. degree in electrical engineering and the Ph.D. degree in automatic control from Lund Institute of Technology, Lund, Sweden, in 1974 and 1979, respectively.

In 1980, he was a Research Associate with the Information Systems Laboratory, Stanford, CA, USA. From 1981 to 1989, he was with Asea Brown Boveri, where he was heavily involved in the introduction of adaptive control in the process industry. In 1989, he was appointed Professor of automatic control with Chalmers University of Technology, Gothenburg, Sweden. His main areas of interest include adaptive and hybrid control and applications of control in the automotive area.

Dr. Egardt has been an Associate Editor of the IEEE TRANSACTIONS ON CONTROL SYSTEMS TECHNOLOGY and the *European Journal of Control*. He is a member of the editorial board of the *International Journal of Adaptive Control and Signal Processing*.